symmetry

MDPI

*Review*

# Applications of Symmetry Breaking in Plasmonics

**Grégory Barbillon [1,*], Andrey Ivanov [2] and Andrey K. Sarychev [2]**

[1] EPF-Ecole d'Ingénieurs, 3 bis rue Lakanal, 92330 Sceaux, France
[2] Institute for Theoretical and Applied Electrodynamics, Russian Academy of Sciences, Moscow 125412, Russia; av.ivanov@physics.msu.ru (A.I.); sarychev@bioplasmonics.com (A.K.S.)
* Correspondence: gregory.barbillon@epf.fr

Received: 25 April 2020; Accepted: 19 May 2020; Published: 1 June 2020


**Abstract:** Plasmonics is one of the most used domains for applications to optical devices, biological and chemical sensing, and non-linear optics, for instance. Indeed, plasmonics enables confining the electromagnetic field at the nanoscale. The resonances of plasmonic systems can be set in a given domain of a spectrum by adjusting the geometry, the spatial arrangement, and the nature of the materials. Moreover, symmetry breaking can be used for the further improvement of the optical properties of the plasmonic systems. In the last three years, great advances in or insights into the use of symmetry breaking in plasmonics have occurred. In this mini-review, we present recent insights and advances on the use of symmetry breaking in plasmonics for applications to chemistry, sensing, devices, non-linear optics, and chirality.

**Keywords:** symmetry breaking; chiral plasmonics; non-linear optics; plasmonic devices; plasmonic sensing

## 1. Introduction

Since the 2000s, the plasmonic nanostructures or nanoparticles have been widely used for realizing optical [1–6] and photovoltaic devices [7–10], as well as sensors of biological and chemical molecules [11–27]. Indeed, these plasmonic systems have different modes such as dipolar resonances [28,29], multipolar resonances [28,29], surface lattice resonances [30], and coupled resonances [31–34]. All these resonances can be set by varying their geometries and the employed materials. Moreover, thanks to the modern tools of fabrication at the nanoscale such as optical and interference lithographies [35–40], focused ion-beam lithography [41], electron-beam lithography [42–45], Nanosphere Lithography (NSL) [46–49], and Nanoimprint Lithography (NIL) [50], the plasmonic systems can be realized by taking into account the different parameters cited above, with an excellent control and accuracy. In addition, another phenomenon can be used for improving the optical properties of plasmonic nanosystems or nanostructures. The latter is symmetry breaking. Indeed, the linear symmetry breaking in plasmonic nanostructures [51,52] has been recently used for studying asymmetric metallic/dielectric metamaterials in order to fabricate photonic devices [53]. To break the symmetry, the structural geometry is modified in order to have an asymmetric system (in-plane or out-of-plane) [54–57]. The alteration of the excitation conditions (light polarization or incidence angle) [58,59] can also induce broken symmetry. Moreover, the effect of the non-linear broken symmetry can be observed as well. For instance, a non-linear symmetry breaking of the Kerr-type has allowed the emergence of a new asymmetric non-linear mode [60]. Other examples of symmetry breaking in non-linear regimes have been observed and studied in non-linear couplers [61] and also in the non-linearity-induced localization of plasmon beams for more sophisticated settings [62].

During these last three years, great advances or insights into the use of symmetry breaking in plasmonics have occurred. Here, an overview of these recent insights and advances on the use of

symmetry breaking in plasmonics is reported. We begin by a review of the applications of symmetry breaking to plasmonic devices. Next, we present the applications to non-linear optics, then those to chiral plasmonics. Finally, a review on the applications of symmetry breaking to chemistry and plasmonic sensing is summarized.

## 2. What Is Symmetry Breaking in Plasmonics?

The symmetry in plasmonic structures strongly affects their optical response. Any structure in gold, silver or another noble metal can be considered as a plasmon antenna where the incident light excites various plasmonic modes. For symmetric metal structures whose size is smaller than the wavelength, the dipolar Electromagnetic (EM) modes prevail. Spatial symmetry breaking induced by the changing of the geometry results in the excitation of other modes [52,54] with much larger local field enhancement since these modes could have small radiation losses. In low symmetry plasmon structures, the incident electromagnetic field achieves so-called dark modes. For instance, symmetry breaking in metallic nanoantenna dimers can induce Fano resonances caused by the interaction of narrow dark modes with broad radiating bright modes [51,52]. In this case, the resonance shape can be tuned by the incidence angle of impinging light. Symmetry breaking reduces degeneracy, and the resonance eigenmodes of the low-symmetry plasmon structures are distributed over all of the frequency space. The scattered field can be always expand in spherical harmonics; however, the coefficients of the expansion have a "geometric" part that can strongly depend on the direction and polarization of the incident light. Non-uniformity of the local field is important for non-linear effects. Another interesting case of symmetry breaking in plasmonics is chiral molecules deposited on a plasmon structure [63]. The plasmon resonance increases the natural chirality, so the whole system loses its symmetry.

## 3. Applications of Symmetry Breaking in Plasmonics

### *3.1. Applications to Plasmonic Devices*

The first field of application for symmetry breaking is plasmonic devices. Several groups have worked on this first application field (see Table 1).

**Table 1.** Improved performances and applications due to symmetry breaking in the field of the plasmonic devices (HMM = Hyperbolic Metamaterials; EP = Exceptional Point).

| Refs. | Improved Performances | Applications |
|---|---|---|
| [64] | Plasmon-induced transparency effect | Biosensing and spectral filters in the terahertz regime |
| [65] | Amplitude control of transmitted light | Security features for anticounterfeiting |
| [66] | Scattering directions | Polarization-dependent security patterns |
| [67] | Tunability of the multimode laser effect | Loss-compensated magnetoplasmonic devices |
| [68] | Polarization-dependent lasing responses | Optical sensing and communications |
| [69] | Optical feedback for nanolasing | Super-resolved imaging and on-chip circuitry |
| [70] | Laser effect with weak scattering | Optofluidic random laser |
| [71] | High transmission efficiency | Photodiodes and single-photon avalanche diodes |
| [72] | Generation of exceptional points | Active components with HMMs and EP |
| [73] | Transverse photo-induced voltage | Photodetection and chiral sensing |
| [74] | Non-Hermicity-induced strong coupling | Localized surface plasmon systems |
| [75] | Reversal of optical binding force | Sensors and particle clustering/aggregation |
| [76] | Optical spectral features | Ultrasensitive biosensing and efficient photocatalysis |

Firstly, Jia et al. reported on obtaining a significant plasmon-induced transparency in THz metamaterials, which can be governed by breaking the structural symmetry [64]. Another example with plasmonic metasurfaces has been investigated where the amplitude and phase of the transmitted signal are controllable by symmetry breaking [65]. In addition, Esposito et al. studied how the symmetry and symmetry breaking of an oligomer allowed the control of the scattering directions [66].

Besides, other groups have demonstrated a laser effect by using symmetry breaking with plasmonic nanostructures such as Ni nanodisc arrays [67], Al nanoparticle arrays [68], and Au nanocrescent arrays [69]. Pourjamal et al. reported on the laser effect (at visible wavelengths) by using ferromagnetic Ni nanodisc arrays on which an organic gain medium was deposited. They observed laser modes (tunable) at different wavelengths by using symmetry breaking of the Ni nanodisc array [67].

Knudson et al. showed polarization-dependent plasmonic lasing responses with rhombohedral arrays of Al anisotropic nanoparticles. When a modification of the excitation beam polarization occurred, the symmetry of the Al nanoparticle array changed (symmetry breaking), and thus, a laser emission wavelength could be selected following the polarization of the pump beam (here, two wavelengths were possible; see Figure 1). The lasing thresholds obtained for these two wavelengths were very similar (see Figure 1d and [68]). Lin et al. described bright quadrupolar lattice plasmon modes obtained for gold nanocrescent arrays that had symmetry breaking could be used as optical feedback for the nanolaser effect. Moreover, if the polarization of the pump beam was changed, the laser effect could be activated or not [69]. Finally, the importance of a replica of broken symmetry was reported for a random laser with weak scattering in an optofluidic environment. The authors remarked that the laser effect coincided with Replica Symmetry Breaking (RSB) and Lévy flight statistics [70].

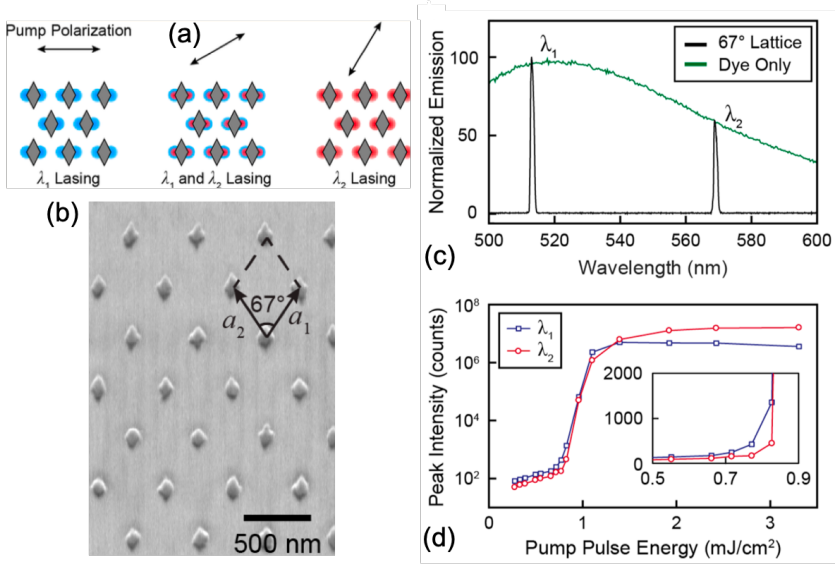


**Figure 1.** (**a**) Principle scheme of lasing at different wavelengths ($\lambda_1$ and $\lambda_2$) depending on the polarization of the pump beam. (**b**) SEM picture of a rhombohedral array of Al nanoparticles displaying the vectors of the lattice. (**c**) Normalized emission spectra for the Al nanoparticle array (lattice angle = 67°) on which dye molecules are deposited (in black) and for only dye molecules (in green). (**d**) Peak intensity versus pump pulse energy for the two wavelengths ($\lambda_1$ in blue and $\lambda_2$ in red). The zoom in (**d**) displays the lasing threshold for the two wavelengths better. All the figures were reprinted (adapted) with permission from [68], Copyright 2019, American Chemical Society.

Besides, Shah et al. showed a high transmission efficiency (44%) with a narrow linewidth (79 nm) from nanohole arrays in a metallic layer. The nanohole shapes used in this study were elliptical and circular, and the organization of the nanoholes was periodic with a periodicity a* (see Figure 2a). They also remarked that this high transmission efficiency was independent of the incidence beam polarization, and the narrow linewidth was caused by an interaction between the extraordinary optical transmission and the Fano resonance. This Fano resonance was realized by symmetry breaking of the nanoholes, which was obtained thanks to the polarization of the impinging beam. Moreover, the experimental transmission peak of 44% observed in Figure 2b is asymmetric, which is characteristic of a Fano resonance (see Figure 2b, the comparison between experiments, and the analytical Fano

lineshape). The experimental result (transmission peak) was in good agreement with the analytical Fano lineshape. Furthermore, from electric field mappings recorded at $\lambda_{peak} = 1642$ nm displayed in Figure 2b, a larger confinement of electric field ($|E|^2$) for elliptical holes was achieved compared to circular holes. Finally, a reflection mode confined within the substrate was observed at $\lambda = 1440$ nm (see Figure 2b and the electric field mapping at 1440 nm for ellipses) [71]. Vaianella et al. investigated the influence of dye molecules integrated in a dielectric medium composed of multilayers of hyperbolic metamaterials. They observed in the regime of strong coupling that strong alterations of plasmonic modes were generated by absorption and emission. These alterations were caused by the splitting of Rabi and the Parity–Time (PT)-symmetry breaking phase with production of Exceptional Points (EP) at certain frequencies [72]. In addition, Akbari et al. reported on the manipulation of the transverse photovoltage obtained with plasmonic triangle holes. This manipulation of the photovoltage (transverse) was elucidated by analyzing the broken symmetry of the mappings of the electric and magnetic fields for plasmonic triangle holes illuminated by a circularly-polarized incident light [73]. Lourenco-Martins et al. demonstrated theoretically and experimentally the strong coupling induced by the non-Hermicity between several plasmonic modes of different orders obtained with silver nanodaggers, which were localized plasmonic systems. This non-Hermicity stemmed from spatial symmetry breaking [74]. Furthermore, the last two examples presented in this mini-review were concerned with the optical properties of plasmonic nanostructures such as spherical heterodimers [75] and tetrahedral nanoparticles [76]. In the first of these two examples, Mahdy et al. reported that the control of the inversion of binding force (here, the force longitudinal component) could be done by varying the light direction or by manipulating its relative orientation with forced symmetry breaking spherical heterodimers [75]. Finally, in the second example, Zheng et al. proved that the tetrahedral shape of a plasmonic nanoparticle, which naturally has symmetry breaking, opens the way toward hybridizations between bright dipolar and quadrupolar modes [76].

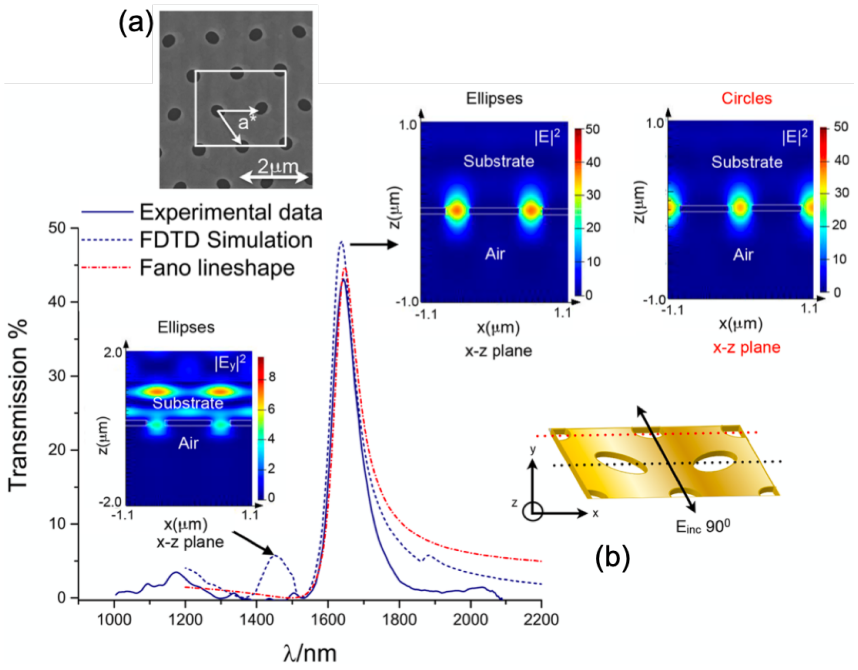


**Figure 2.** (**a**) SEM picture of periodic nanoholes. a* corresponds to the periodicity. (**b**) Comparison between experiments, FDTD simulations, and the analytical Fano lineshape for $E_{inc} = 90°$. From electric field mappings recorded at $\lambda_{peak} = 1642$ nm, $|E|^2$ for elliptical holes is larger than $|E|^2$ for circular holes. From the electric field mapping recorded at $\lambda = 1440$ nm, a reflection within the substrate is displayed. All the figures were reprinted (adapted) with permission from [71], Copyright 2018, American Chemical Society.

### 3.2. Applications to Non-Linear Optics

The second field of application for symmetry breaking is non-linear optics. Several groups have demonstrated that symmetry breaking can improve the optical performances of plasmonic systems applied to non-linear optics (see Table 2).

**Table 2.** Improved performances and applications due to symmetry breaking in the field of non-linear optics (SHG = Second Harmonic Generation; FWM = Four-Wave Mixing; TDMC = Transition Metal Dichalcogenides; SRR = Split-Ring Resonator; SFG = Sum Frequency Generation).

| Refs. | Improved Performances | Applications |
|---|---|---|
| [77] | Polarization-dependent SHG signals | Detection of the symmetry of nanostructures/molecules |
| [78] | SHG and FWM non-linear processes | Identification of the role of high-order antenna modes |
| [79] | Second-order non-linear susceptibilities | Creation and active tuning of second-order non-linearities |
| [80] | Plasmon-enhanced SHG of TDMCs | Ideal integration platform for on-chip non-linear plasmonics |
| [81] | SHG of vertical SRRs | Photonics and sensing |
| [82] | SFG signals | Spectroscopic analysis and sensing of molecules |

For instance, Rahmani et al. demonstrated that a novel type of non-linear broken symmetry in plasmonic nanosystems (oligomers) was observed by analyzing the Second Harmonic Generation (SHG) variations due to the change of the angle of impinging light polarization (see Figure 3). Figure 3 shows a scheme of the nanostructures investigated in this paper with the excitation conditions and also the SHG intensity versus the azimuthal angle of the linear polarization for the excitation light. This approach can enable the detection of the symmetry of oligomers or other molecules [77].

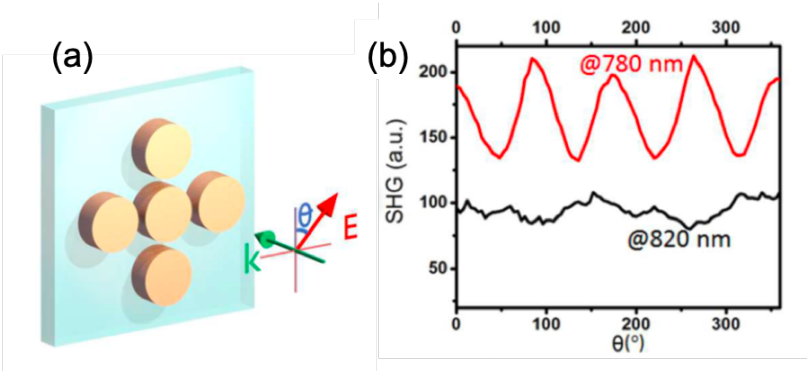


**Figure 3.** (**a**) Scheme of the studied pentamer on a glass substrate with the excitation conditions. (**b**) SHG intensity versus the azimuthal angle of the excitation polarization (in red, $\lambda_{exc}$ = 780 nm, and in black, $\lambda_{exc}$ = 820 nm). All the figures were reprinted (adapted) with permission from [77], Copyright 2017, American Chemical Society.

In addition, Gennaro et al. investigated the significance of higher order modes of antennas with metasurfaces having a non-linear gradient (broken symmetry) and based on the Pancharatnam–Berry phase by using SHG and Four-Wave Mixing (FWM) non-linear signals. They demonstrated that generalized diffraction rules (for the geometric phase) were found taking into account the higher order modes and the structural rotation in order to extend the geometric phase metasurfaces to non-linear signals with a broken symmetry [78]. Another different example of applications is the creation and the active control of second-order non-linearities as the second-order non-linear susceptibility $\chi^{(2)}$. Indeed, Taghinejad et al. demonstrated that inversion symmetry breaking by using hot-electron dynamics could be employed in order to have an all-optical tuning of effective responses for $\chi^{(2)}$. In this study, a hybrid system composed of an Au triangle on an amorphous $TiO_2$ film was used for conversion under the picosecond of an inactive dielectric material into a transient non-linear medium thanks to an ultrafast transfer of hot electrons [79]. Besides, Shi et al. observed a significant enhancement (∼400) of

the SHG signal by using a monolayer of Transition Metal Dichalcogenides (TMDCs; here tungsten disulfide $WS_2$) integrated on a silver nanogroove grating. One of the optical properties of TDMCs is a significant second-order non-linearity, which has a broken inversion symmetry in 2D crystals. However, this non-linearity is limited by a sub-nanometric thickness. Thus, this monolayer of $WS_2$ is deposited on plasmonic nanogrooves spatially arranged in a grating in order to enhance the SHG signal. The surface plasmon in nanogrooves is excited in a such way that the SHG frequency is in resonance with the C-exciton of the $WS_2$ film. The SHG enhancement is due to the significant electric field confinement in the nanogrooves [80].

In the following two examples, symmetry breaking inducing modifications of non-linear optical properties is dedicated to the sensing of molecules. For the first example, Tsai et al. demonstrated an enhancement factor of 2.6 for the SHG non-linearity obtained with vertical Split-Ring Resonators (vertical SRRs = U-shaped nanostructures of which the basis of U is only on the glass substrate; see more details in [81]) compared to the planar SRRs. In this study, plasmonic SRRs had geometries with broken centro-symmetries at the level of the interface between air and the plasmonic surface. This enhancement of the SHG signal was due to the fact that vertical SRRs could lift the localized fields (electric and magnetic) of surface plasmons, which were confined between the two vertical arms and did not "touch" the glass substrate [81]. In the second example, Dalstein et al. observed an improvement of the non-linear optical signal called Sum Frequency Generation (SFG) for gold spherical nanoparticles coated with dodecanethiol molecules by red-shifting the visible wavelength of excitation (see Figure 4). This enhancement was due to the plasmonic coupling involved in the SFG phenomenon when the excitation wavelength located in the visible spectral domain was red-shifted, and the fact that strong electric fields and a broken symmetry related to hotspots created in nanoparticle multimers (or aggregates) were involved in the plasmonic coupling, even if the presence of multimers or aggregates of Au nanospheres was weak [82]. Figure 4 displays a SEM image of gold nanospheres on Si substrate, where we observe a couple of multimers or aggregates. Then, SFG spectra recorded at 20 visible wavelengths of excitation are presented, and finally SFG intensity is displayed versus excitation wavelength. Indeed, from the SFG spectra displayed in Figure 4b,c, an increase of the SFG signal was observed when the visible wavelength of excitation was red-shifted, as explained previously.

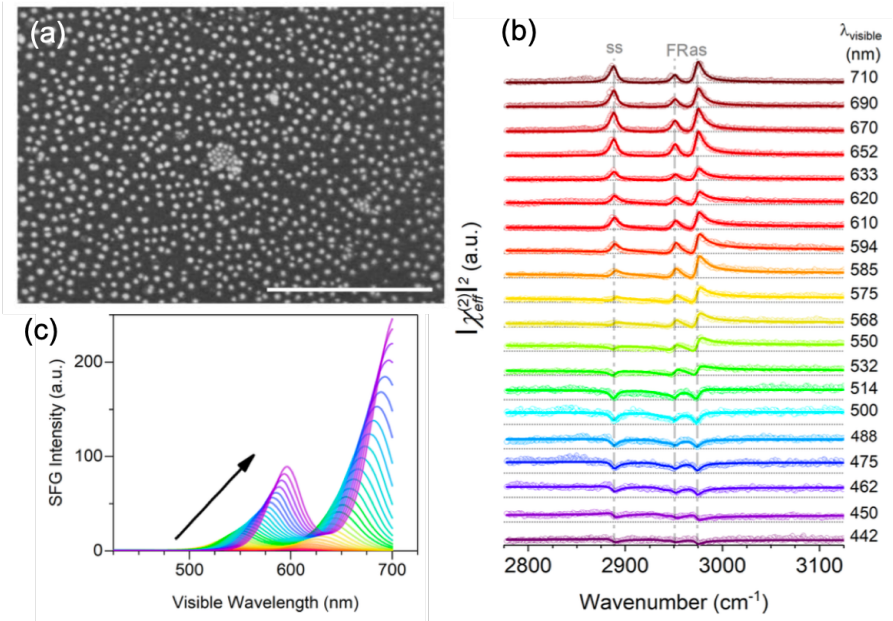


**Figure 4.** (**a**) SEM picture of Au nanospheres on Si substrate (scale bar = 500 nm). (**b**) SFG spectra recorded at 20 visible wavelengths of excitation (from 442 nm to 710 nm). (**c**) SFG intensity versus the visible wavelength of excitation. All the figures were reprinted (adapted) with permission from [82], Copyright 2019, American Chemical Society.

### *3.3. Applications to Chiral Plasmonics*

The third field of application for symmetry breaking is chiral plasmonics. A couple of groups reported on chiral plasmonic nanostructures with symmetry breaking (see Table 3) such as Au nanorod equilateral trimers [83], chiral metamaterials composed of plasmonic slanted nanoapertures [84], plasmonic Λ-shaped nanostructures [85], plasmonic ramp-shaped nanostructures [86], 3D plasmonic crescents [87], and GaAS/Au nanowires [88].

**Table 3.** Improved performances and applications due to symmetry breaking in the field of chiral plasmonics.

| Refs. | Improved Performances | Applications |
|---|---|---|
| [83] | Hybridized plasmon modes | Optical magnetic field enhancement |
| [84] | Circular dichroism in transmission | Chiral imaging, sensing, and spectroscopy |
| [85] | 3D chiral effects | Study of complex plasmonic nanostructures |
| [86] | Circular dichroism | Nanoscale circular polarizers |
| [87] | Tailoring of circular dichroism | Chiral sensing and circular dichroism spectroscopy |
| [88] | Circular dichroism | Chiral sensing devices |

In the first example, the bidimensional chiral effect was approached. Greybush et al. demonstrated that gold nanorod assemblies (see the examples in Figure 5a) enabled obtaining hybrid plasmonic modes, which were dependent on rotation and polarization. These hybrid plasmonic modes were also sensitive to the changes of the size, position, and orientation of gold nanorods that were conducive to the symmetry breaking of the geometry. The hybrid plasmonic modes (resonances) were characterized by using dark-field scattering spectroscopy under excitation for which the Polarization was Left-Circular (LCP) or Right-Circular (RCP) (see Figure 5b). The chiroptical response of gold nanorod assemblies was obtained by determining the percent of the Circular Differential Scattering (%CDS; see Figure 5c), which depended on the scattering intensities under LCP excitation and RCP excitation [83]. Figure 5b,c displays the scattering spectra with LCP and RCP excitation in which several peaks appear indicating a privileged excitation conducive to a "bisignate" lineshape of which the values of the chiroptical response %CDS could be negative or positive.

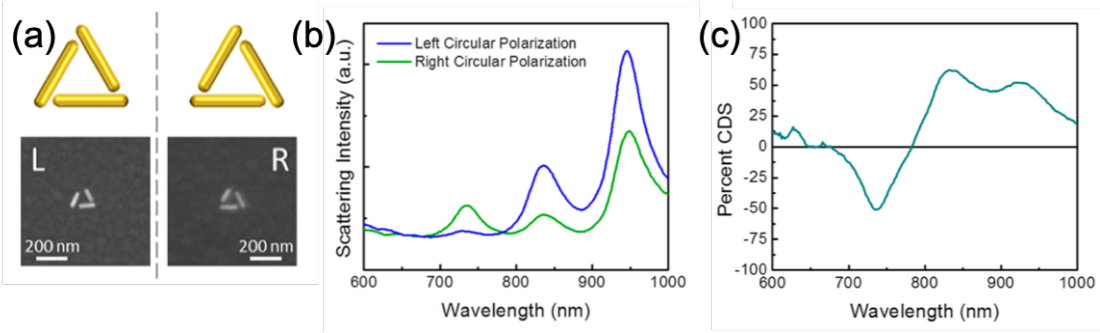


**Figure 5.** (**a**) Scheme and SEM pictures of a nanorod trimer oriented "at the left" (L) and oriented "at the right" (R). (**b**) Experimental scattering spectra for the trimer oriented "at the right" illuminated with a left circular (in blue) polarization and a right circular (in green) polarization of the excitation beam. (**c**) Circular Differential Scattering (CDS) versus the wavelength obtained with the scattering data of (**b**). All the figures were reprinted (adapted) with permission from [83], Copyright 2019, American Chemical Society.

Now, we report on the tridimensional chiral effect. Chen et al. reported on a novel design of chiral metamaterials based on the tilt of nanoapertures along a given direction (see Figure 6a,b) in order to break all the symmetries. This novel design consisted of slanted split-ring nanoapertures (SSRA) and allowed obtaining a giant Circular Dichroism in Transmission (CDT) in the spectral range

of the near-infrared (78% at 760 nm; see Figure 6c), which depended on Transmissions recorded with a Left-Circular (T-LCP) or Right-Circular Polarization (T-RCP) of incident light. Moreover, this giant CDT came from a mode coupling between portions of the waveguide within slanted nanoapertures [84].

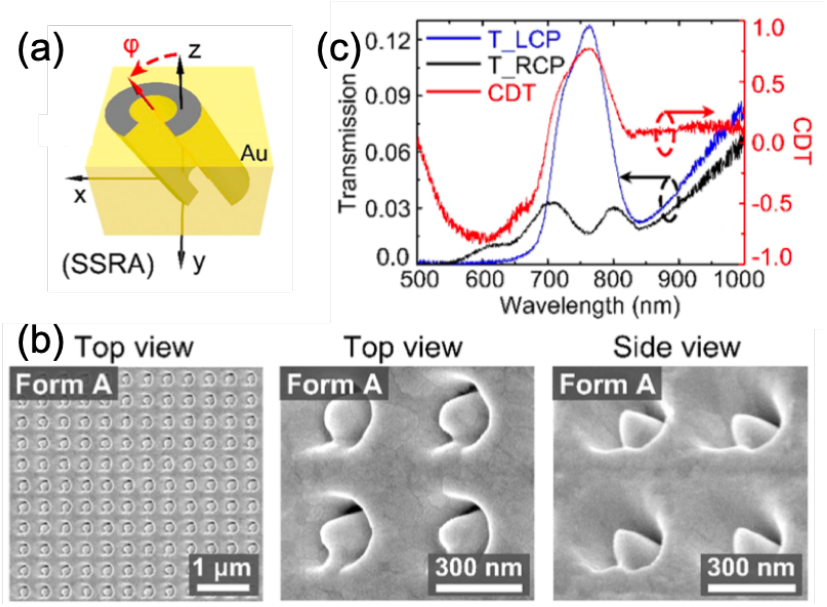


**Figure 6.** (**a**) Scheme of a slanted split-ring nanoaperture (SSRA). (**b**) SEM pictures of SSRA in Form A with an inclination angle of 40°. (**c**) Experimental spectra of transmission for SSRA (in Form A) with Transmissions recorded with a Left-Circular (T-LCP) (in blue color) or Right-Circular Polarization (T-RCP) (in black color) of incident light and the corresponding spectrum of Circular Dichroism in Transmission (CDT, in red color). All the figures were reprinted (adapted) with permission from [84], Copyright 2018, American Chemical Society.

Pham et al. demonstrated 3D chiral effects in Λ-shaped plasmonic nanoapertures due to the defects of symmetry breaking [85]. Besides, Rajaei et al. showed that the gradient depth for a plasmonic array of nanostructures with a ramp shape provided symmetry breaking that led to a significant value of the Circular Dichroism (CD) in the range of visible frequencies (CD = 64% at the wavelength of 678 nm) obtained by reflection spectroscopy [86]. Furthermore, Goerlitzer et al. showed the fabrication of 3D plasmonic crescents with tuning of chirality by using on-edge colloidal lithography. Indeed, the chirality could be tuned experimentally by moving the position of the deposition step of a silicon dioxide film on which metallic crescent-shaped structures were realized. This intermediate film of silicon dioxide permitted symmetry breaking of the crescent structure [87]. To finish this part on chiral plasmonics, Leahu et al. reported on the fabrication of GaAs/AlGaAs/GaAS nanowires partially overlayed with gold, which led to symmetry breaking and thus a chiral response (circular dichroism) [88].

### *3.4. Applications to Chemistry and Plasmonic Sensing*

To finish this mini-review, the last fields of application presented here are chemistry and plasmonic sensing (see Table 4). The first four examples are devoted to chemistry [89–92], and the last six are dedicated to plasmonic sensing [93–98].

**Table 4.** Improved performances and applications due to symmetry breaking in the field of chemistry and plasmonic sensing (NP = Nanoparticle; EP = Exceptional Point).

| Refs. | Improved Performances | Applications |
|---|---|---|
| [89] | Plasmonic resonances | Surface-enhanced Raman scattering sensing |
| [90] | Splitting of plasmon modes | Sensing |
| [91] | Optical properties of 1D plasmonic nanostructures | Solution-phase metamaterials |
| [92] | Dynamic process of $H_2$ dissociation on metallic NP | Tunable photochemistry |
| [93] | Splitting of plasmon modes for alloy nanodisc arrays | Biosensing technologies |
| [94] | Detection sensitivity | Modern biosensors |
| [95] | Magnetic Fano resonances | Bioanalytics via high precision sensing |
| [96] | Detection sensitivity with plasmonic EPs | Nanoscale devices and sensors |
| [97] | Circular dichroism | Detection of chiral molecules |
| [98] | Circular dichroism | Chiral sensors |

In the first study, Topal et al. investigated the plasmonic modes in silver Nanohemispheres (NHSs) using an incident illumination with an *s*- and *p*-polarization for different angles. They showed that symmetry breaking by the shape of asymmetric nanoparticles (nanohemispheres) was conducive to dipole modes, which were parallel and also normal to the base. These dipole modes were extremely distinct in terms of electromagnetic coupling, energy, and dependence on polarization for the excitation. For instance, the principal parallel mode provided a couple of advantages in plasmonics compared to the classical case of nanospheres. Indeed, the very intense coupling of a parallel mode with the substrate gave the possibility of benefiting photovoltaics in thin films through an efficient coupling of light [89]. Furthermore, Smith et al. proved that the degenerated plasmonic modes of gold nanotriangles were responsive to symmetry breaking. Indeed, they demonstrated that the inclination of Au nanotriangles led to a substantial breaking of the degeneracy between plasmonic modes [90]. In addition, Jones et al. studied the optical properties of plasmonic nanostructures realized by using assembly by DNA, allowing a deterministic symmetry breaking. The symmetry breaking enabled the emergence of coupled modes of the $\pi$-type constituted by both dipolar and quadripolar modes [91]. To finish the applications to chemistry, Zhang et al. showed the dynamic process of $H_2$ dissociation on plasmonic nanoparticles (see Figure 7a), which was a plasmonic chemical process obtained by the intermediary of hot-carriers. Indeed, this process took place when the $H_2$ molecule was near to a unique plasmonic nanoparticle. When the $H_2$ molecule was situated at an equal distance between the two nanoparticles forming the dimer, the suppression of the $H_2$ dissociation occurred on account of a sequential charge transfer (see Figure 7a,b). If the $H_2$ molecule were moved asymmetrically in this gap, then the symmetry was broken, and the $H_2$ dissociation was restored due to the meaningful stop of the additional charge transfer (see Figure 7a,b). From Figure 7c, no dissociation occurred for this case where D = d = 5.82 Å(gray line). Moreover, this case was identically sensitive to that with D = d = 1.59 Å(green line). The only difference between these two cases was that the scale of the bond-fluctuation time was quicker for the case D = d = 5.82 Å. For the given distance D between the nanoparticle and the molecule of dihydrogen, the dissociation effectively started when the size d of the dimer exceeded some critical value $d_c$. It is interesting to note that the distance $d_c$ for the effective $H_2$ dissociation increased when the resonance energy $\omega$ increased [92].

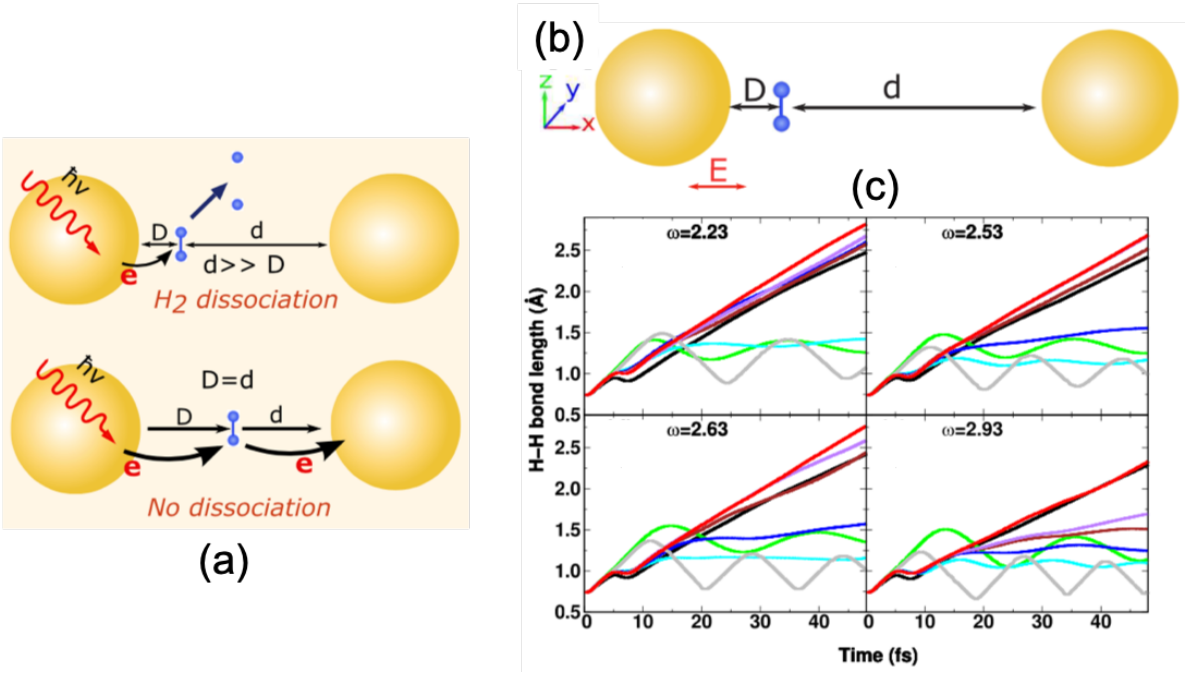


**Figure 7.** (**a**) Principle scheme of the dissociation of the $H_2$ molecule within a dimer. (**b**) Scheme of the configuration used for the case where $H_2$ is placed between the plasmonic nanoparticles, and the distance D is set at 1.59 Å. The other distance is d, which is not fixed. (**c**) Bond dynamics of $H_2$ within the dimer for several distances d (with D = 1.59 Å) for four resonant energies ($\omega$): in black, for a monomer, for d = 1.59, 3.70, 5.82, 7.94, 10.05, 12.17 Å(in green, cyan, blue, brown, purple, red, respectively), and for the last case, in grey, for D = d = 5.82 Å. All the figures were reprinted (adapted) with permission from [92], Copyright 2018, American Chemical Society.

In the first example dedicated to plasmonic sensing, Misbah et al. showed the mode splitting induced by symmetry breaking for coupled Au-Ag Alloy Nanodisc Arrays (ANAs; see Figure 8a). In this ANA, two modes, of which one had low energy and the other had High Energy (HE mode), appeared due to the splitting of the original plasmonic mode of a single nanodisc. The resonance of the HE mode could be set at 540 nm by using alloy nanodiscs that were rich in silver. Then, the authors used this mode obtained with an ANA coupled in the far-field, because this mode was related to a higher sensitivity to local refractive index variations (344 nm/RIU; RIU = Refractive Index Unit) compared to classical plasmonic arrays for the same spectral range. This same mode was also of key significance for colorimetric sensing. By using this mode, the detection limit was $10^{-10}$ M for the concentration of streptavidin (see Figure 8b), a molecule used for testing these plasmonic ANAs, and for this same concentration, the Red/Green (R/G) ratio reduction was slightly inferior to 0.05 (see Figure 8b) [93].

Furthermore, Zhu et al. demonstrated that symmetry breaking of the 3D metallic nanoholes improved the sensitiveness to local refractive index changes up to 946 nm/RIU. This effect was due to the improvement of the electric field localized on corners, and the excitation of a supplemental plasmonic quadrupolar mode. Then, the authors demonstrated 3D Plasmonic Photonic Crystal (PPC) nanostructures, which were obtained from quasi-3D plasmonic nanoholes on which quasi-3D SU-8 nanosquares were reverse-imprinted in order to sustain gold nanosquares on the top. These gold nanosquares broke the symmetry of the quasi-3D plasmonic nanoholes. This mixture allowed a better EM field confinement from the spatial point of view. Moreover, they improved their 3D PPC by introducing point-defect cavities in order to enhance the confinement of the EM field around the defect zones. Thus, with this type of nanostructure, the sensitivity to local refractive index changes was 1376 nm/RIU. A detection limit of $10^4$ particles per mL for the concentration of exosomes was obtained, characterized by a spectral shift of 9 nm for the resonance peak at 1082 nm [94]. Next, Wang et al.

investigated symmetric nanotrimer arrays with a high density in the infrared domain in order to obtain magnetic Fano resonances induced by symmetry breaking. The authors showed that the excitation of these resonances could occur when a coupling between neighboring cells involved a broken symmetry. The latter showed a sensitivity to local refractive index variations of around 300 nm/RIU [95]. Park et al. demonstrated that the refractive index sensitivity for plasmonic exceptional points was 4821 nm/RIU and enabled the detection of $15 \times 10^{-12}$ g·L$^{-1}$ for the concentration of anti-immunoglobulin G. The plasmonic exceptional points were found on the hybridized detuned resonators in a bilayered plasmon periodic edifice. The critical complex coupling led to the fusion of both losses and resonances. The broken symmetry performed the detuning by employing alike resonators within dissimilar optical media [96]. To finish this part on plasmonic sensing, a couple of groups demonstrated a plasmon-enhanced sensing of the chiral molecules [97,98]. In this case, the plasmon resonance of nanostructures increased the natural chirality of molecules so the whole system lost its symmetry. Indeed, the highly confined electromagnetic fields of plasmonic structures allowed a better interaction between these fields and chiral molecules, which were deposited on these plasmonic structures.

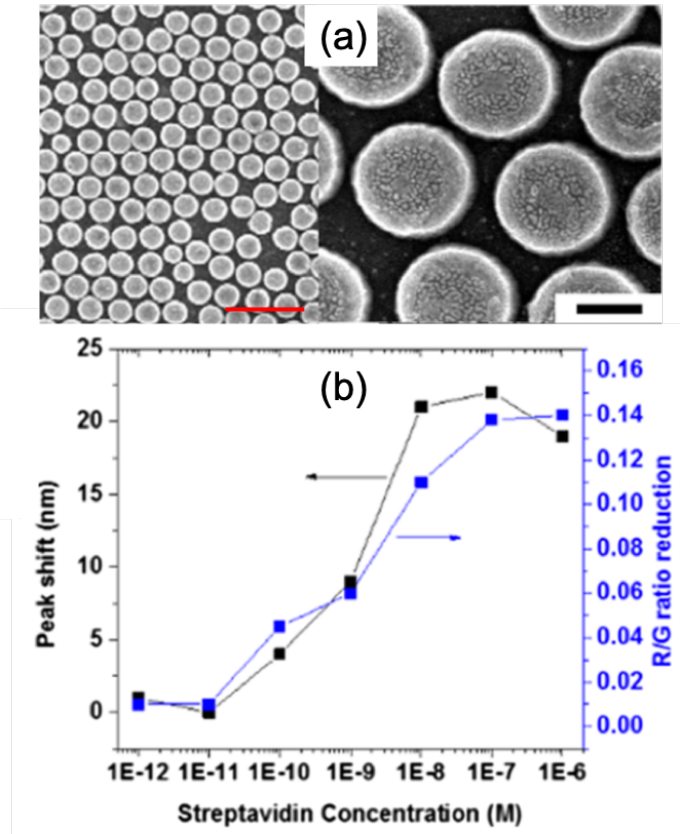


**Figure 8.** (**a**) SEM pictures of an alloy nanodisc array (scale bar = 1000 nm, and for the zoom, scale bar = 200 nm). (**b**) Spectral shift of the resonance peak at 540 nm (in black) and the Red/Green (R/G) ratio reduction (in blue) versus streptavidin concentration. All the figures were reprinted (adapted) with permission from [93], Copyright 2019, American Chemical Society.

## 4. Conclusions

In this mini-review, recent insights and advances concerning the applications of symmetry breaking in plasmonics were reported in four major parts: (i) plasmonic devices, (ii) non-linear optics, (iii) chiral plasmonics, and (iv) chemistry and plasmonic sensing. Indeed, symmetry breaking has a key role in many physical and chemical phenomena. In general, symmetry breaking is employed in order to enhance different properties or effects of plasmonic nanostructures such as transmission efficiency, nanolasing, second harmonic generation signals, sum frequency generation signals, circular dichroism,

splitting of plasmonic modes, sensitivity to local refractive index changes for sensing applications, and $H_2$ dissociation. Thus, symmetry breaking is a phenomenon that is not to be neglected and to be used for a great number of fields such as those cited previously, for instance.

**Author Contributions:** G.B. wrote the whole paper, prepared the original draft, and edited the draft; A.I. wrote Section 2 and edited the draft; A.K.S. wrote Section 2 and edited the draft. All authors have read and agreed to the published version of the manuscript.

**Funding:** This research was partially supported by the Russian Science Foundation (Grant No. 16-14-00209).

**Conflicts of Interest:** The authors declare no conflict of interest.

## References

1. Haffner, C.; Heni, W.; Fedoryshyn, Y.; Niegemann, J.; Melikyan, A.; Elder, D.L.; Baeuerle, B.; Salamin, Y.; Josten, A.; Koch, U.; et al. All-plasmonic Mach-Zehnder modulator enabling optical high-speed communication at the microscale. *Nat. Photonics* **2015**, *9*, 525–528. [CrossRef]
2. Ayata, M.; Fedoryshyn, Y.; Heni, W.; Baeuerle, B.; Josten, A.; Zahner, M.; Koch, U.; Salamin, Y.; Hoessbacher, C.; Haffner, C.; et al. High-speed plasmonic modulator in a single metal layer. *Science* **2017**, *358*, 630–632. [CrossRef] [PubMed]
3. Magno, G.; Bélier, B.; Barbillon, G. Gold thickness impact on the enhancement of SERS detection in low-cost Au/Si nanosensors. *J. Mater. Sci.* **2017**, *52*, 13650–13656. [CrossRef]
4. Salamin, Y.; Ma, P.; Baeuerle, B.; Emboras, A.; Fedoryshyn, Y.; Heni, W.; Cheng, B.; Josten, A.; Leuthold, J. 100 GHz Plasmonic Photodetector. *ACS Photonics* **2018**, *5*, 3291–3297. [CrossRef]
5. Thomaschewski, M.; Yang, Y.Q.; Bozhevolnyi, S.I. Ultra-compact branchless plasmonic interferometers. *Nanoscale* **2018**, *10*, 16178–16183. [CrossRef]
6. Sarychev, A.K.; Ivanov, A.; Lagarkov, A.; Barbillon, G. Light Concentration by Metal-Dielectric Micro-Resonators for SERS Sensing. *Materials* **2019**, *12*, 103. [CrossRef]
7. Chen, X.; Fang, J.; Zhang, X.D.; Zhao, Y.; Gu, M. Optical/Electrical Integrated Design of Core-Shell Aluminum-Based Plasmonic Nanostructures for Record-Breaking Efficiency Enhancements in Photovoltaic Devices. *ACS Photonics* **2017**, *4*, 2102–2110. [CrossRef]
8. Li, M.Z.; Guler, U.; Li, Y.A.; Rea, A.; Tanyi, E.K.; Kim, Y.; Noginov, M.A.; Song, Y.L.; Boltasseva, A.; Shalaev, V.M.; et al. Plasmonic Biomimetic Nanocomposite with Spontaneous Subwavelength Structuring as Broadband Absorbers. *ACS Energy Lett.* **2018**, *3*, 1578–1583. [CrossRef]
9. Shao, W.J.; Liang, Z.Q.; Guan, T.F.; Chen, J.M.; Wang, Z.F.; Wu, H.H.; Zheng, J.Z.; Abdulhalim, I.; Jiang, L. One-step integration of a multiple-morphology gold nanoparticle array on a $TiO_2$ film via a facile sonochemical method for highly efficient organic photovoltaics. *J. Mater. Chem. A* **2018**, *6*, 8419–8429. [CrossRef]
10. Vangelidis, I.; Theodosi, A.; Beliatis, M.J.; Gandhi, K.K.; Laskarakis, A.; Patsalas, P.; Logothetidis, S.; Silva, S.R.P.; Lidorikis, E. Plasmonic Organic Photovoltaics: Unraveling Plasmonic Enhancement for Realistic Cell Geometries. *ACS Photonics* **2018**, *5*, 1440–1452. [CrossRef]
11. Pichon, B.P.; Barbillon, G.; Marie, P.; Pauly, M.; Begin-Colin, S. Iron oxide magnetic nanoparticles used as probing agents to study the nanostructure of mixed self-assembled monolayers. *Nanoscale* **2011**, *3*, 4696–4705. [CrossRef] [PubMed]
12. He, Y.; Su, S.; Xu, T.T.; Zhong, Y.L.; Zapien, J.A.; Li, J.; Fan, C.H.; Lee, S.T. Silicon nanowires-based highly-efficient SERS-active platform for ultrasensitive DNA detection. *Nano Today* **2011**, *6*, 122–130. [CrossRef]
13. Huang, J.-A.; Zhao, Y.-Q.; Zhang, X.-J.; He, L.-F.; Wong, T.-L.; Chui, Y.-S.; Zhang, W.-J.; Lee, S.-T. Ordered Ag/Si Nanowires Array: Wide-Range Surface-Enhanced Raman Spectroscopy for Reproducible Biomolecule Detection. *Nano Lett.* **2013**, *13*, 5039–5045. [CrossRef] [PubMed]
14. Dalstein, L.; Ben Haddada, M.; Barbillon, G.; Humbert, C.; Tadjeddine, A.; Boujday, S.; Busson, B. Revealing the Interplay between Adsorbed Molecular Layers and Gold Nanoparticles by Linear and Nonlinear Optical Properties. *J. Phys. Chem. C* **2015**, *119*, 17146–17155. [CrossRef]
15. Bryche, J.-F.; Bélier, B.; Bartenlian, B.; Barbillon, G. Low-cost SERS substrates composed of hybrid nanoskittles for a highly sensitive sensing of chemical molecules. *Sens. Actuators B* **2017**, *239*, 795–799. [CrossRef]

16. Tian, X.; Lin, Y.; Dong, J.; Zhang, Y.; Wu, S.; Liu, S.; Zhang, Y.; Li, J.; Tian, Z. Synthesis of Ag Nanorods with Highly Tunable Plasmonics toward Optimal Surface-Enhanced Raman Scattering Substrates Self-Assembled at Interfaces. *Adv. Opt. Mater.* **2017**, *5*, 1700581. [CrossRef]
17. Chen, J.; Gan, F.; Wang, Y.; Li, G. Plasmonic Sensing and Modulation Based on Fano Resonances. *Adv. Opt. Mater.* **2018**, *6*, 1701152. [CrossRef]
18. Dolci, M.; Bryche, J.-F.; Leuvrey, C.; Zafeiratos, S.; Gree, S.; Begin-Colin, S.; Barbillon, G.; Pichon, B.P. Robust clicked assembly based on iron oxide nanoparticles for a new type of SPR biosensor. *J. Mater. Chem. C* **2018**, *6*, 9102–9110. [CrossRef]
19. Lu, G.; Xu, J.; Wen, T.; Zhang, W.; Zhao, J.; Hu, A.; Barbillon, G.; Gong, Q. Hybrid Metal-Dielectric Nano-Aperture Antenna for Surface Enhanced Fluorescence. *Materials* **2018**, *11*, 1435. [CrossRef]
20. Magno, G.; Bélier, B.; Barbillon, G. Al/Si nanopillars as very sensitive SERS substrates. *Materials* **2018**, *11*, 1534. [CrossRef]
21. Barbillon, G. Fabrication and SERS Performances of Metal/Si and Metal/ZnO Nanosensors: A Review. *Coatings* **2019**, *9*, 86. [CrossRef]
22. Humbert, C.; Noblet, T.; Dalstein, L.; Busson, B.; Barbillon, G. Sum-Frequency Generation Spectroscopy of Plasmonic Nanomaterials: A Review. *Materials* **2019**, *12*, 836. [CrossRef] [PubMed]
23. Zambrana-Puyalto, X.; Ponzellini, P.; Maccaferri, N.; Tessarolo, E.; Pelizzo, M.G.; Zhang, W.; Barbillon, G.; Lu, G.; Garoli, D. A hybrid metal-dielectric zero mode waveguide for enhanced single molecule detection. *Chem. Commun.* **2019**, *55*, 9725–9728. [CrossRef] [PubMed]
24. Barbillon, G.; Ivanov, A.; Sarychev, A.K. Hybrid Au/Si Disk-Shaped Nanoresonators on Gold Film for Amplified SERS Chemical Sensing. *Nanomaterials* **2019**, *9*, 1588. [CrossRef] [PubMed]
25. Graniel, O.; Iatsunskyi, I.; Coy, E.; Humbert, C.; Barbillon, G.; Michel, T.; Maurin, D.; Balme, S.; Miele, P.; Bechelany, M. Au-covered hollow urchin-like ZnO nanostructures for surface-enhanced Raman scattering sensing. *J. Mater. Chem. C* **2019**, *7*, 15066–15073. [CrossRef]
26. Tomyshev, K.A.; Tazhetdinova, D.K.; Manuilovich, E.S.; Butov, O.V. High-resolution fiber optic surface plasmon resonance sensor for biomedical applications. *J. Appl. Phys.* **2018**, *124*, 113106. [CrossRef]
27. Cai, S.S.; Gonzalez-Vila, A.; Zhang, X.J.; Guo, T.; Caucheteur, C. Palladium-coated plasmonic optical fiber gratings for hydrogen detection. *Opt. Lett.* **2019**, *44*, 4483–4486. [CrossRef]
28. Maier, S.A. *Plasmonics: Fundamentals and Applications*; Springer: New York, NY, USA, 2007; pp. 3–220.
29. Enoch, S.; Bonod, N. *Plasmonics: From Basics to Advanced Topics*; Springer: Heidelberg, Germany, 2012; pp. 3–317.
30. Kravets, V.G.; Kabashin, A.V.; Barnes, W.L.; Grigorenko, A.N. Plasmonic Surface Lattice Resonances: A Review of Properties and Applications. *Chem. Rev.* **2018**, *118*, 5912–5951. [CrossRef]
31. Li, Z.; Butun, S.; Aydin, K. Ultranarrow Band Absorbers Based on Surface Lattice Resonances in Nanostructured Metal Surfaces. *ACS Nano* **2014**, *8*, 8242–8248. [CrossRef]
32. Sarkar, M.; Besbes, M.; Moreau, J.; Bryche, J.-F.; Olivéro, A.; Barbillon, G.; Coutrot, A.-L.; Bartenlian, B.; Canva, M. Hybrid Plasmonic Mode by Resonant Coupling of Localized Plasmons to Propagating Plasmons in a Kretschmann Configuration. *ACS Photonics* **2015**, *2*, 237–245. [CrossRef]
33. Sobhani, A.; Manjavacas, A.; Cao, Y.; McClain, M.J.; Javier Garcia de Abajo, F.; Nordlander, P.; Halas, N.J. Pronounced Linewidth Narrowing of an Aluminum Nanoparticle Plasmon Resonance by Interaction with an Aluminum Metallic Film. *Nano Lett.* **2015**, *15*, 6946–6951. [CrossRef] [PubMed]
34. Yue, W.; Wang, Z.; Whittaker, J.; Lopez-Royo, F.; Yang, Y.; Zayats, A.V. Amplification of surface-enhanced Raman scattering due to substrate-mediated localized surface plasmons in gold nanodimers. *J. Mater. Chem. C* **2017**, *5*, 4075–4084. [CrossRef]
35. Barbillon, G.; Bijeon, J.-L.; Lérondel, G.; Plain, J.; Royer, P. Detection of chemical molecules with integrated plasmonic glass nanotips. *Surf. Sci.* **2008**, *602*, L119–L122. [CrossRef]
36. Dhawan, A.; Duval, A.; Nakkach, M.; Barbillon, G.; Moreau, J.; Canva, M.; Vo-Dinh, T. Deep UV nano-microstructuring of substrates for surface plasmon resonance imaging. *Nanotechnology* **2011**, *22*, 165301. [CrossRef] [PubMed]
37. Zhang, P.; Yang, S.; Wang, L.; Zhao, J.; Zhu, Z.; Liu, B.; Zhong, J.; Sun, X. Large-scale uniform Au nanodisc arrays fabricated via X-ray interference lithography for reproducible and sensitive SERS substrate. *Nanotechnology* **2014**, *25*, 245301. [CrossRef]

38. Guisbert Quilis, N.; Lequeux, M.; Venugopalan, P.; Khan, I.; Knoll, W.; Boujday, S.; Lamy de la Chapelle, M.; Dostalek, J. Tunable laser interference lithography preparation of plasmonic nanoparticle arrays tailored for SERS. *Nanoscale* **2018**, *10*, 10268. [CrossRef]
39. Hwang, J.S.; Yang, M. Sensitive and Reproducible Gold SERS Sensor Based on Interference Lithography and Electrophoretic Deposition. *Sensors* **2018**, *18*, 4076. [CrossRef]
40. Hentschel, M.; Schäferling, M.; Duan, X.; Giessen, H.; Liu, N. Chiral plasmonics. *Sci. Adv.* **2017**, *3*, e1602735. [CrossRef]
41. Henzie, J.; Lee, J.; Lee, M.H.; Hasan, W.; Odom, T.W. Nanofabrication of Plasmonic Structures. *Annu. Rev. Phys. Chem.* **2009**, *60*, 147–165. [CrossRef]
42. Yu, Q.; Guan, P.; Qin, D.; Golden, G.; Wallace, P.M. Inverted size-dependence of surface-enhanced Raman scattering on gold nanohole and nanodisc arrays. *Nano Lett.* **2008**, *8*, 1923–1928. [CrossRef]
43. Faure, A.C.; Barbillon, G.; Ou, M.; Ledoux, G.; Tillement, O.; Roux, S.; Fabregue, D.; Descamps, A.; Bijeon, J.-L.; Marquette, C.A.; et al. Core/shell nanoparticles for multiple biological detection with enhanced sensitivity and kinetics. *Nanotechnology* **2008**, *19*, 485103. [CrossRef] [PubMed]
44. Bryche, J.-F.; Gillibert, R.; Barbillon, G.; Sarkar, M.; Coutrot, A.-L.; Hamouda, F.; Aassime, A.; Moreau, J.; de La Chapelle, M.L.; Bartenlian, B.; et al. Density effect of gold nanodiscs on the SERS intensity for a highly sensitive detection of chemical molecules. *J. Mater. Sci.* **2015**, *50*, 6601–6607. [CrossRef]
45. Sarychev, A.K.; Bykov, I.V.; Boginskaya, I.A.; Ivanov, A.V.; Kurochkin, I.N.; Lagarkov, A.N.; Nechaeva, N.L.; Ryzhikov, I.A. Metal-dielectric optical resonance in metasurfaces and SERS effect. *Opt. Quantum Electron.* **2020**, *52*, 26. [CrossRef]
46. Masson, J.F.; Gibson, K.F.; Provencher-Girard, A. Surface-enhanced Raman spectroscopy amplification with film over etched nanospheres. *J. Phys. Chem. C* **2010**, *114*, 22406–22412. [CrossRef]
47. Bechelany, M.; Brodard, P.; Elias, J.; Brioude, A.; Michler, J.; Philippe, L. Simple Synthetic Route for SERS-Active Gold Nanoparticles Substrate with Controlled Shape and Organization. *Langmuir* **2010**, *26*, 14364–14371. [CrossRef] [PubMed]
48. Bryche, J.-F.; Tsigara, A.; Bélier, B.; Lamy de la Chapelle, M.; Canva, M.; Bartenlian, B.; Barbillon, G. Surface enhanced Raman scattering improvement of gold triangular nanoprisms by a gold reflective underlayer for chemical sensing. *Sens. Actuators B* **2016**, *228*, 31–35. [CrossRef]
49. Barbillon, G.; Noblet, T.; Busson, B.; Tadjeddine, A.; Humbert, C. Localised detection of thiophenol with gold nanotriangles highly structured as honeycombs by nonlinear sum frequency generation spectroscopy. *J. Mater. Sci.* **2018**, *53*, 4554–4562. [CrossRef]
50. Ding, T.; Sigle, D.O.; Herrmann, L.O.; Wolverson, D.; Baumberg, J.J. Nanoimprint lithography of Al Nanovoids for Deep-UV SERS. *ACS Appl. Mater. Interfaces* **2014**, *6*, 17358–17363. [CrossRef]
51. Luk'yanchuk, B.; Zheludev, N.I.; Maier, S.A.; Halas, N.J.; Nordlander, P.; Giessen, H.; Chong, C.T. The Fano resonance in plasmonic nanostructures and metamaterials. *Nat. Mater.* **2010**, *9*, 707–715. [CrossRef]
52. Halas, N.J.; Lal, S.; Chang, W.-S.; Link, S.; Nordlander, P. Plasmons in strongly coupled metallic nanostructures. *Chem. Rev.* **2011**, *111*, 3913–3961. [CrossRef]
53. Durach, M.; Rusina, A.; Stockman, M.I.; Nelson, K. Toward full spatiotemporal control on the nanoscale. *Nano Lett.* **2007**, *7*, 3145–3149. [CrossRef]
54. Hao, F.; Sonnefraud, Y.; Dorpe, P.V.; Maier, S.A.; Halas, N.J.; Nordlander, P. Symmetry breaking in plasmonic nanocavities: subradiant LSPR sensing and a tunable Fano resonance. *Nano Lett.* **2008**, *8*, 3983–3988. [CrossRef]
55. Liu, N.; Hentschel, M.; Weiss, T.; Alivisatos, A.P.; Giessen, H. Three-dimensional plasmon rulers. *Science* **2011**, *332*, 1407–1410. [CrossRef] [PubMed]
56. Kondratov, A.V.; Gorkunov, M.V.; Darinskii, A.N.; Gainutdinov, R.V.; Rogov, O.Y.; Ezhov, A.A.; Artemov, V.V. Extreme optical chirality of plasmonic nanohole arrays due to chiral Fano resonance. *Phys. Rev. B* **2016**, *93*, 195418. [CrossRef]
57. Dietrich, K.; Menzel, C.; Lehr, D.; Puffky, O.; Hübner, U.; Pertsch, T.; Tünnermann, A.; Kley, E.-B. Elevating optical activity: Efficient on-edge lithography of three-dimensional starfish metamaterial. *Appl. Phys. Lett.* **2014**, *104*, 193107. [CrossRef]
58. Camacho-Morales, R.; Rahmani, M.; Kruk, S.; Wang, L.; Xu, L.; Smirnova, D.A.; Solntsev, A.S.; Miroshnichenko, A.; Tan, H.H.; Karouta, F.; et al. Nonlinear generation of vector beams from AlGaAs nanoantennas. *Nano Lett.* **2016**, *16*, 7191–7197. [CrossRef]

59. Hao, F.; Nordlander, P.; Sonnefraud, Y.; Dorpe, P.V.; Maier, S.A. Tunability of subradiant dipolar and Fano-type plasmon resonances in metallic ring/disk cavities: implications for nanoscale optical sensing. *ACS Nano* **2009**, *3*, 643–652. [CrossRef]
60. Davoyan, A.R.; Shadrivov, I.V.; Kivshar, Y.S. Nonlinear plasmonic slot waveguides. *Opt. Express* **2008**, *16*, 21209–21214. [CrossRef]
61. Salgueiro, J.R.; Kivshar, Y.S. Nonlinear plasmonic directional couplers. *Appl. Phys. Lett.* **2010**, *97*, 081106. [CrossRef]
62. Kravtsov, V.; Ulbricht, R.; Atkin, J.M.; Raschke, M.B. Plasmonic nanofocused four-wave mixing for femtosecond near-field imaging. *Nat. Nanotechnol.* **2016**, *11*, 459–464. [CrossRef]
63. Nesterov, M.L.; Yin, X.; Schäferling, M.; Giessen, H.; Weiss, T. The role of Plasmon-Generated Near Fields for Enhanced Circular Dichroism Spectroscopy. *ACS Photonics* **2016**, *3*, 578–583. [CrossRef]
64. Jia, W.; Ren, P.; Jia, Y.; Fan, C. Active Control and Large Group Delay in Graphene-Based Terahertz Metamaterials. *J. Phys. Chem. C* **2019**, *123*, 18560–18564. [CrossRef]
65. Frese, D.; Wei, Q.; Wang, Y.; Huang, L.; Zentgraf, T. Nonreciprocal Asymmetric Polarization Encryption by Layered Plasmonic Metasurfaces. *Nano Lett.* **2019**, *19*, 3976–3980. [CrossRef] [PubMed]
66. Esposito, M.; Todisco, F.; Bakhti, S.; Passaseo, A.; Tarantini, I.; Cuscuna, M.; Destouches, N.; Tasco, V. Symmetry Breaking in Oligomer Surface Plasmon Lattice Resonances. *Nano Lett.* **2019**, *19*, 1922–1930. [CrossRef] [PubMed]
67. Pourjamal, S.; Hakala, T.K.; Necada, M.; Freire-Fernandez, F.; Kataja, M.; Rekola, H.; Martikainen, J.; Törmä, P.; van Dijken, S. Lasing in Ni Nanodisk Arrays. *ACS Nano* **2019**, *13*, 5686–5692. [CrossRef]
68. Knudson, M.P.; Li, R.; Wang, D.; Wang, W.; Schaller, R.D.; Odom, T.W. Polarization-Dependent Lasing Behavior from Low-Symmetry Nanocavity Arrays. *ACS Nano* **2019**, *13*, 7435–7441. [CrossRef]
69. Lin, Y.; Wang, D.; Hu, J.; Liu, J.; Wang, W.; Guan, J.; Schaller, R.D.; Odom, T.W. Engineering Symmetry-Breaking Nanocrescent Arrays for Nanolasing. *Adv. Funct. Mater.* **2019**, *29*, 1904157. [CrossRef]
70. Sarkar, A.; Shivakiran Bhaktha, B.N.; Andreasen, J. Replica Symmetry Breaking in a Weakly Scattering Optofluidic Random Laser. *Sci. Rep.* **2020**, *10*, 2628. [CrossRef]
71. Shah, Y.D.; Grant, J.; Hao, D.; Kenney, M.; Pusino, V.; Cumming, D.R.S. Ultra-narrow Line Width Polarization-Insensitive Filter Using a Symmetry-Breaking Selective Plasmonic Metasurface. *ACS Photonics* **2018**, *5*, 663–669. [CrossRef]
72. Vaianella, F.; Hamm, J.M.; Hess, O.; Maes, B. Strong Coupling and Exceptional Points in Optically Pumped Active Hyperbolic Metamaterials. *ACS Photonics* **2018**, *5*, 2486–2495. [CrossRef]
73. Akbari, M.; Gao, J.; Yang, X. Manipulating transverse photovoltage across plasmonic triangle holes of symmetry breaking. *Appl. Phys. Lett.* **2019**, *114*, 171102. [CrossRef]
74. Lourenço-Martins, H.; Das, P.; Tizei, L.H.G.; Weil, R.; Kociak, M. Self-hybridization within non-Hermitian localized plasmonic systems. *Nat. Phys.* **2018**, *14*, 360–364. [CrossRef]
75. Mahdy, M.R.C.; Danesh, M.; Zhang, T.; Ding, W.; Rivy, H.M.; Chowdhury, A.B.; Mehmood, M.Q. Plasmonic Spherical Heterodimers: Reversal of Optical Binding Force Based on the Forced Breaking of Symmetry. *Sci. Rep.* **2018**, *8*, 3164. [CrossRef] [PubMed]
76. Zheng, P.; Paria, D.; Wang, H.; Li, M.; Barman, I. Optical properties of symmetry-breaking tetrahedral nanoparticles. *Nanoscale* **2020**, *12*, 832–842. [CrossRef] [PubMed]
77. Rahmani, M.; Shorokhov, A.S.; Hopkins, B.; Miroshnichenko, A.E.; Shcherbakov, M.R.; Camacho-Morales, R.; Fedyanin, A.A.; Neshev, D.N.; Kivshar, Y.S. Nonlinear Symmetry Breaking in Symmetric Oligomers. *ACS Photonics* **2017**, *4*, 454–461. [CrossRef]
78. Gennaro, S.D.; Li, Y.; Maier, S.A.; Oulton, R.F. Nonlinear Pancharatnam–Berry Phase Metasurfaces beyond the Dipole Approximation. *ACS Photonics* **2019**, *6*, 2335–2341. [CrossRef]
79. Taghinejad, M.; Xu, Z.; Lee, K.-T.; Lian, T.; Cai, W. Transient Second-Order Nonlinear Media: Breaking the Spatial Symmetry in the Time Domain via Hot-Electron Transfer. *Phys. Rev. Lett.* **2020**, *124*, 013901. [CrossRef]
80. Shi, J.; Liang, W.-Y.; Raja, S.; Sang, Y.; Zhang, X.-Q.; Chen, C.-A.; Wang, Y.; Yang, X.; Lee, Y.-H.; Ahn, H.; et al. Plasmonic Enhancement and Manipulation of Optical Nonlinearity in Monolayer Tungsten Disulfide. *Laser Photonics Rev.* **2018**, *12*, 1800188. [CrossRef]

81. Tsai, W.-Y.; Chung, T.L.; Hsiao, H.-H.; Chen, J.-W.; Lin, R.J.; Wu, P.C.; Sun, G.; Wang, C.-M.; Misawa, H.; Tsai, D.P. Second Harmonic Light Manipulation with Vertical Split Ring Resonators. *Adv. Mater.* **2019**, *31*, 1806479. [CrossRef]
82. Dalstein, L.; Humbert, C.; Ben Haddada, M.; Boujday, S.; Barbillon, G.; Busson, B. The Prevailing Role of Hotspots in Plasmon-Enhanced Sum-Frequency Generation Spectroscopy. *J. Phys. Chem. Lett.* **2019**, *10*, 7706–7711. [CrossRef]
83. Greybush, N.J.; Pacheco-Pena, V.; Engheta, N.; Murray, C.B.; Kagan, C.R. Plasmonic Optical and Chiroptical Response of Self-Assembled Au Nanorod Equilateral Trimers. *ACS Nano* **2019**, *13*, 1617–1624. [CrossRef] [PubMed]
84. Chen, Y.; Gao, J.; Yang, X. Chiral Metamaterials of Plasmonic Slanted Nanoapertures with Symmetry Breaking. *Nano Lett.* **2018**, *18*, 520–527. [CrossRef] [PubMed]
85. Pham, A.; Jiang, Q.; Zhao, A.; Bellessa, J.; Genet, C.; Drezet, A. Manifestation of Planar and Bulk Chirality Mixture in Plasmonic Λ-Shaped Nanostructures Caused by Symmetry Breaking Defects. *ACS Photonics* **2017**, *4*, 2453–2460. [CrossRef]
86. Rajaei, M.; Zeng, J.; Albooyeh, M.; Kamandi, M.; Hanifeh, M.; Capolino, F.; Wickramasinghe, H.K. Giant Circular Dichroism at Visible Frequencies Enabled by Plasmonic Ramp-Shaped Nanostructures. *ACS Photonics* **2019**, *6*, 924–931. [CrossRef]
87. Goerlitzer, E.S.A.; Mohammadi, R.; Nechayev, S.; Banzer, P.; Vogel, N. Large-Area 3D Plasmonic Crescents with Tunable Chirality. *Adv. Optical Mater.* **2019**, *7*, 1801770. [CrossRef]
88. Leahu, G.; Petronijevic, E.; Belardini, A.; Centini, M.; Sibilia, C.; Hakkarainen, T.; Koivusalo, E.; Piton, M.R.; Suomalainen, S.; Guina, M. Evidence of Optical Circular Dichroism in GaAs-Based Nanowires Partially Covered with Gold. *Adv. Opt. Mater.* **2017**, *5*, 1601063. [CrossRef]
89. Özge Topal, Ç.; Jaradat, H.M.; Karumuri, S.; O'Hara, J.F.; Akyurtlu, A.; Kaan Kalkan, A. Plasmon Resonances in Nanohemisphere Monolayers. *J. Phys. Chem. C* **2017**, *121*, 23599–23608. [CrossRef]
90. Smith, K.W.; Yang, J.; Hernandez, T.; Swearer, D.F.; Scarabelli, L.; Zhang, H.; Zhao, H.; Moringo, N.A.; Chang, W.-S.; Liz-Marzan, L.M.; et al. Environmental Symmetry Breaking Promotes Plasmon Mode Splitting in Gold Nanotriangles. *J. Phys. Chem. C* **2018**, *122*, 13259–13266. [CrossRef]
91. Jones, M.R.; Kohlstedt, K.L.; O'Brien, M.N.; Wu, J.; Schatz, G.C.; Mirkin, C.A. Deterministic Symmetry Breaking of Plasmonic Nanostructures Enabled by DNA-Programmable Assembly. *Nano Lett.* **2017**, *17*, 5830–5835. [CrossRef]
92. Zhang, Y.; Nelson, T.; Tretiak, S.; Guo, H.; Schatz, G.C. Plasmonic Hot-Carrier-Mediated Tunable Photochemical Reactions. *ACS Nano* **2018**, *12*, 8415–8422. [CrossRef]
93. Misbah, I.; Zhao, F.; Shih, W.-C. Symmetry Breaking-Induced Plasmonic Mode Splitting in Coupled Gold–Silver Alloy Nanodisk Array for Ultrasensitive RGB Colorimetric Biosensing. *ACS Appl. Mater. Interfaces* **2019**, *11*, 2273–2281. [CrossRef] [PubMed]
94. Zhu, S.; Li, H.; Yang, M.; Pang, S.W. Highly sensitive detection of exosomes by 3D plasmonic photonic crystal biosensor. *Nanoscale* **2018**, *10*, 19927–19936. [CrossRef] [PubMed]
95. Wang, N.; Zeisberger, M.; Huebner, U.; Giannini, V.; Schmidt, M.A. Symmetry-breaking induced magnetic Fano resonances in densely packed arrays of symmetric nanotrimers. *Sci. Rep.* **2019**, *9*, 2873. [CrossRef] [PubMed]
96. Park, J.; Ndao, A.; Cai, W.; Hsu, L.; Kodigala, A.; Lepetit, T.; Lo, Y.; Kanté, B. Symmetry-breaking-induced plasmonic exceptional points and nanoscale sensing. *Nat. Phys.* **2020**, *16*, 462–468. [CrossRef]
97. Zhang, W.; Wu, T.; Wang, R.; Zhang, X. Surface-Enhanced Circular Dichroism of Oriented Chiral Molecules by Plasmonic Nanostructures. *J. Phys. Chem. C* **2017**, *121*, 666–675. [CrossRef]
98. Garcia-Guirado, J.; Svedendahl, M.; Puigdollers, J.; Quidant, R. Enantiomer-Selective Molecular Sensing Using Racemic Nanoplasmonic Arrays. *Nano Lett.* **2018**, *18*, 6279–6285. [CrossRef]